PHYSICAL REVIEW A **81**, 031401(R) (2010)

Three-dimensional lattice of ion traps

K. Ravi,[1] Seunghyun Lee,[1] Arijit Sharma,[1] Tridib Ray,[1] G. Werth,[2] and S. A. Rangwala[1,*]
[1]*Raman Research Institute, Sadashivanagar, Bangalore 560080, India*
[2]*Institut für Physik, Johannes-Gutenberg-Universität, D-55099 Mainz, Germany*
(Received 26 June 2009; published 4 March 2010)

We propose an ion trap configuration that, by symmetry, is three-dimensionally frequency degenerate. This fundamental trap configuration can be stacked together in a three-dimensional simple cubic arrangement. The isolated trap, as well as the extended array of ion traps, is characterized for different locations in the lattice, illustrating the robustness of the lattice of traps concept. The ease of addressing the ions at each lattice site, individually or simultaneously, makes this system naturally suitable for a number of experiments. Application of this trap to precision spectroscopy, quantum information processing, and the study of few-particle interacting systems are discussed.

DOI: 10.1103/PhysRevA.81.031401 PACS number(s): 37.10.Ty, 03.67.−a, 29.30.Ep, 95.55.Sh

The trapping of ions with static [1] and time-varying [2] fields has been central to many important developments in physics and chemistry for the past 50 years. Ion traps have been applied to precision spectroscopy [1], precision mass determination [3], mass analysis [4], atomic ion clocks [5], and, most recently, quantum information processing [6]. Ion trap experiments most typically focus on the ability to trap (a) a single ultracold ion for extended interrogation, (b) a collection of ions in the form of a spatially extended cloud [7], or (c) an ordered crystal of ions [8,9]. Multiple species of ions can also be trapped simultaneously [10]. Common to all of these experiments is the study of ion(s) within isolated ion traps. Recently experiments have been performed to communicate between trapped ions in remote experiments [11]. Different trap configurations have been developed to meet specific requirements, starting from conventional 3-dimensional (3-D) traps with hyperbolic electrodes [2] to cylindrical traps [12], linear traps [13], and various kinds of planar traps [14–17]. Designs with 3-D scalability [18,19] and ion transport [20] have also been explored.

In this article we propose a configuration for ion trapping which is three-dimensionally symmetric by its geometry. It resembles the configuration used by Wuerker *et al.* [21] in 1959. An important consequence of the present structure is its suitability for the construction of several compact, stacked, virtually independent ion traps in the same apparatus. Here we discuss the fundamental structure underlying the proposed trap and its operating scheme. Parameters for both the isolated fundamental trap and the system of stacked traps are determined and compared, establishing the robustness of the configuration. The motion of ions in the traps is characterized, building a case for several experimental applications with this trapping scheme, some of which are sketched to illustrate its versatility.

The fundamental building block for the lattice of ion traps (LIT) is illustrated in Fig. 1(a). The trap is constructed with three parallel pairs of cylindrical electrodes along the Cartesian axes. When extended, this creates compact, well-isolated individual traps with large optical access, permitting optical communication between different traps and ease of construction. Typical dimensions could be an electrode diameter of 0.5 mm and a center-to-center separation of 5 mm. These are the dimensions used in our simulations. The dimensions can be changed without qualitatively changing the characterization here.

Time-varying potentials create the 3-D ion trap, when applied to the equipotential, parallel electrodes in Fig. 1(a). The phase relation for the amplitude of the applied radio-frequency (RF) field between electrode sets along $\hat{x}$, $\hat{y}$, and $\hat{z}$ is illustrated in Fig. 1(b). This field configuration creates the rotating saddle potential which traps the ions in a 3-D symmetric configuration over one full cycle of the rf. This symmetry lends itself to extension, to form the LIT illustrated in Fig. 1(c). In general any $l \times m \times n$ number of equivalent traps can be constructed by building an appropriate number of electrodes. The rf phase relation remains identical to the fundamental trap for the extended sets of parallel electrodes. Figure 1(c) illustrates the $3 \times 3 \times 3$ version of the LIT, as it is the lowest-order cubic arrangement that provides lattice sites with differently located near-neighbor traps (coordination). The four distinct locations of ion traps in this arrangement are body center (BC), face center (FC), edge center (EC), and corner (C). We show here that the site-specific effects on the trapped ions in individual traps are too small to be significant.

The ion trap operation is simulated for the $^{40}Ca^{+}$ ion. The potentials for the ion trap(s) are generated using SIMION. The equations of motion in the time-varying potentials are solved numerically using MATHEMATICA. The rotating saddle potential results in ion motion with a macromotion frequency ν_m whose amplitude is modulated by the driving frequency of the trap, ν_{rf}. Characterization simulations for the isolated ion trap and the LIT potential were done by solving for the full $3 \times 3 \times 3$ cell configuration. The isolated trap solutions were then compared with the corresponding solutions within the individual traps at the BC, FC, EC, and C locations.

Operationally, apart from the dimensions of the trap, three parameters characterize the symmetric 3-D ion trap. These are frequency (ν_{rf}) of operation, amplitude of the rf (V_{rf}), and trap depth for the ion. Equal amplitudes of the rf voltage V_{rf} applied as in Fig. 1(b) yield macromotion frequencies $\nu_{m;x} = \nu_{m;y} = \nu_{m;z}$. No dc field is applied to the electrodes in our trap

*sarangwala@rri.res.in

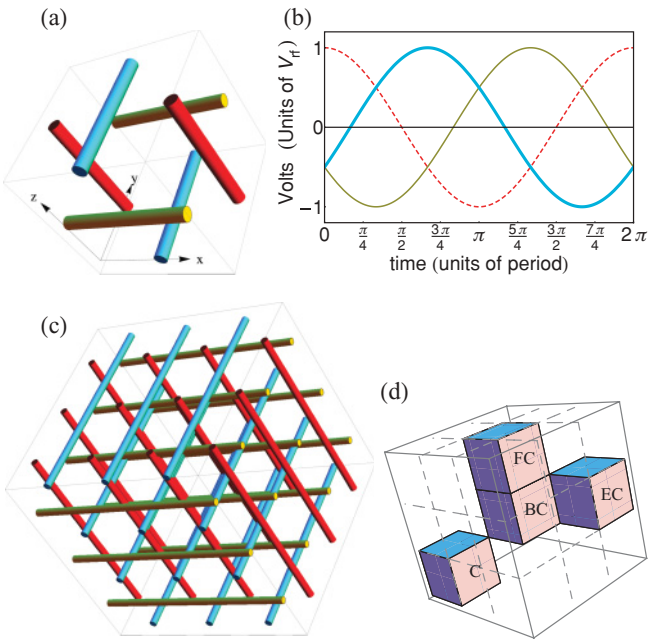

FIG. 1. (Color online) Structure and operation of the 3-D ion trap. (a) Basic electrode configuration of the ion trap. Three pairs of parallel electrodes are arranged along the Cartesian axes and are electrically contacted. (b) The relative phase difference of $2\pi/3$ between the orthogonal electrode sets, where V_x, V_y, and V_z are represented by thin, thick, and dashed lines, respectively. (c) Illustration of the extension of the trap in (a) to 27 traps in a simple cubic arrangement. (d) Four distinct types of coordination symmetries for traps at different locations emerge. Representative cells of different coordinations are identified as BC(6), FC(5), EC(4), and C(3), where the number of location-dependent nearest-neighbor cells is given in parentheses.

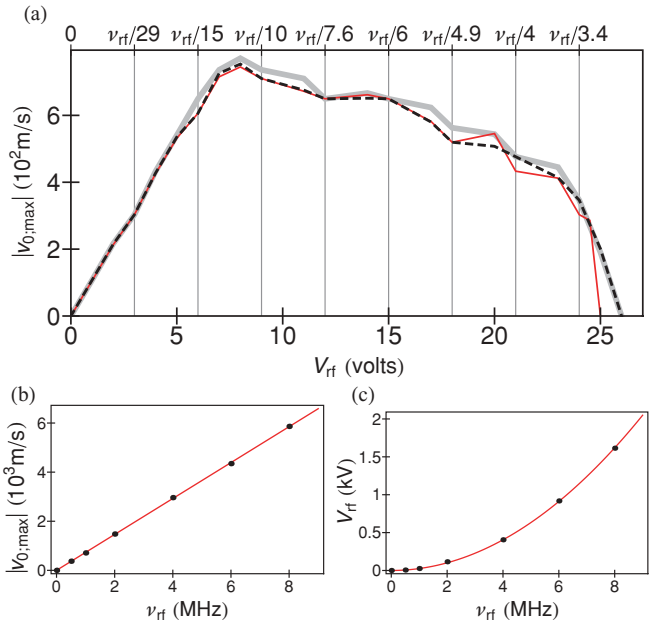

FIG. 2. (Color online) Details of trap characterization. (a) Region of stability in the $|\mathbf{v}_0|$ vs. V_{rf} plane at $\nu_{rf} = 1$ MHz. The region contained within the curve is the stable region. The dashed (black), thin (red), and thick (gray) lines are the stability bounds for the single trap in Fig. 1(a), the most configurationally distinct BC, and C cells in the LIT, respectively. (b) Plot of the maximum initial velocity that is trapped $|\mathbf{v}_{0;max}|$ and (c) plot of the maximum amplitude of the rf field which traps the $^{40}Ca^+$ ion as a function of ν_{rf}. The line is the least-squares fit to the points, $\alpha\nu_{rf}$ for (b) and $\beta\nu_{rf}^2$ for (c).

configuration. As a consequence of this, the standard Paul trap representation in terms of stability parameters a and q, related to the Mathieu differential equation, which governs the motion of ions in a rf trap [2], is not relevant, as $a = 0$. However,

$$q = 4QV_{rf}/M(2\pi\nu_{rf})^2R_0^2,$$

where Q represents the charge state of the ion, M the mass, and $R_0 = 0.0025$ m the distance of the electrode from the trap center; that is, the size of the trap, remains a good expression for trap characterization.

The nature of the present trap is characterized by relating the rf amplitude V_{rf}, the magnitude of the initial velocity of the trapped ion $|\mathbf{v}_0|$, and ν_{rf}. Figure 2(a) illustrates the boundary of the region of stability in the $|\mathbf{v}_0|$-V_{rf} plane, where $\nu_{rf} = 1$ MHz, for the single trap, BC, and C locations. The initial position of the ion is at the trap center and the initial velocity is $\mathbf{v}_0$, with equal components in the three orthogonal directions. The small variations in the trapping region in Fig. 2(a) arise due to the trapping potential at the edge of the physical trap. A barely trapped ion samples the outer reaches of the individual trap potential, where, in addition to intrinsic anharmonicity, the trap at its edges is susceptible to its immediate neighborhood. Thus the differences due to the trap location in the LIT are minor. The top axis in Fig. 2(a) marks out the macromotion frequency ν_m as a fraction of ν_{rf} for the isolated trap and is dependent only on the magnitude of V_{rf}. As V_{rf} increases, the amplitude of the micromotion increases rapidly, thus taking the ions to the trap boundary and ejecting them. Deeper trap potentials therefore do not imply higher initial kinetic energies of trappable ions, as illustrated by the fall in the $|\mathbf{v}_{0;max}|$ for higher V_{rf} values. Thus the suitable operating point of the ion trap is the initial region of linear response of $|\mathbf{v}_{0;max}|$ to V_{rf}, with $q \leqslant 0.29$ for $V_{rf} \leqslant 8$ V at $\nu_{rf} = 1$ MHz. Generating multiple $|\mathbf{v}_0|$-V_{rf} stability plots for different ν_{rf} and compiling the results provided the data for Figs. 2(b) and (c). Figure 2(b) illustrates that $|\mathbf{v}_{0;max}|$ scales as ν_{rf}, quantifying the maximum trappable initial velocity of the ion. Figure 2(c) demonstrates that the maximum trapping voltage $V_{rf;max}$ scales as ν_{rf}^2 consistent with the behavior for constant q, here $q = 0.908$, which barely traps the zero-velocity ion. Thus the bounds for the operation of the present ion trap are well characterized via the scaling functions shown.

Symmetric operation of the trap gives identical macromotion frequency ν_m, in the orthogonal $\hat{x}$, $\hat{y}$, and $\hat{z}$ direction. The micromotion of the trajectory components is synchronous with the drive field frequency ν_{rf}. At the trap center and for a large range of $|\mathbf{v}_0|$, ν_m is unchanged and the power spectrum in Fig. 3 remains free of sidebands, indicating that the trap is harmonic. Due to the large difference between ν_m and ν_{rf} in the $q \leqslant 0.29$ range of operation, it is reasonable to separate the ion motion into two components, and the slow motion at ν_m can be considered separate, while averaging over the fast oscillation at ν_{rf}. This is indeed exhibited clearly in the amplitude of the power spectrum of the Fourier transform

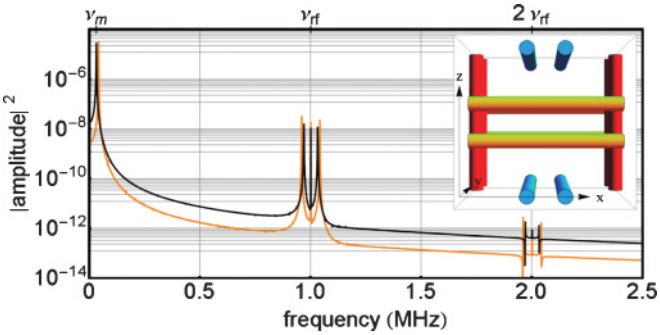

FIG. 3. (Color online) Power spectrum of the $\hat{x}$ component of the trajectory for a low-$|\mathbf{v}_0|$ ion computed at $\nu_{rf} = 1$ MHz, $V_{rf} = 3$ V: (i) for the electrode configuration in Fig. 1(a), black curve, and (ii) for the split electrode configuration in the inset, gray (orange) trace. For both power spectra, a strong macromotion peak at ν_m and significantly weaker peaks at ν_{rf}, $\nu_{rf} \pm \nu_m$, $2\nu_{rf}$, and $2\nu_{rf} \pm \nu_m$ are seen.

along the representative $\hat{x}$ direction in Fig. 3. In the small-$\mathbf{v}_0$ and low-q region of operation, ν_m is the same across traps with different coordination numbers.

The absolute uncertainty in ν_m determination from our simulations is within $\pm 0.01\nu_{rf}$. This uncertainty arises due to a marginal deviation of the the numerical solution to the Laplace equation from the true value of the potential because of our computational convergence limit.

Structurally the electrodes of the trap illustrated in Figs. 1(a) and 1(c) do not allow a face-on view of the ion. This can be circumvented by splitting each of the six electrodes into two closely spaced electrodes as shown in the inset in Fig. 3. The resulting trap is similar in performance to the trap in Fig. 1(a), as illustrated in Fig. 3 by the power spectrum of the $\hat{x}$ component of the ion trajectory.

Loading the LIT with the desired number of ions is most efficiently achieved by resonance-enhanced two-photon ionization. Briefly, the rf fields could be applied while a vapor of the parent neutral floods the lattice. Application of the two laser frequencies participating in the ionization, along two distinct directions of easy viewing through the lattice, would create ions only at the beam intersection. Thus an ion(s) can be loaded in a controlled way in each ion trap cell, close to the center of the individual traps. Laser cooling of ions to ultracold temperatures, now well established, is easily done along the easy viewing directions.

The proposed ion trap, due to the sinusoidal, three-phase variation of the solution of the Laplace equations, is tightly constrained by the uniqueness theorems. Alternative configurations of ion traps which yield degenerate frequencies with sinusoidal time variation (Fig. 3, inset) will be qualitatively identical to the trap above. It is also found that the trap degeneracies are preserved for small trap misalignments, while a 3% deviation in electrode placement leads to a breakdown of the frequency degeneracy. The optical access (OA) at the center of the trap in Fig. 1(a) is OA $\approx 0.81 \times (4\pi)$ sr, while the central trap in the LIT has OA $\approx 0.58 \times (4\pi)$ sr. This makes the addressing of ions in the LIT practical.

The most precise spectroscopic measurement on a system would be on an isolated, trapped single particle, nearly at rest. However, in the specific case of a single ion confined within an ion trap, a serious constraint is presented by the low flux of the photons and hence the signal-to-noise ratio ($\mathcal{R}_{S/N}$) in the detection. Adding more than one ion per ion trap leaves the system vulnerable to perturbations that could compromise the precision of the measured transition frequencies. With the experimental setup proposed here, we have the ability to preserve the isolation of the individual ions in each trap, while increasing the detected fluorescence rate.

Specifically the performance of single-ion optical clocks may be improved when a single ultracold ion is trapped within each cell of the LIT. The stability of clocks is expressed by the Allen variance,

$$\sigma = (\Delta\nu/\nu)(\mathcal{R}_{S/N})^{-1/2} \times \tau^{-1/2},$$

where ν is the transition frequency, $\Delta\nu$ is the observed linewidth, and τ is the integration time. In the arrangement illustrated in Fig. 1(c), 27 such trapped ions can be interrogated simultaneously, increasing the $\mathcal{R}_{S/N}$. This results in a decrease in the short-term instability by about a factor of 5.

Information processing with ion traps allows the most precise control over qubits thus far. However, one practical limitation faced by most ion trap quantum information experiments is scalability and, to an extent, precise individual addressing of the ions trapped in the ground vibrational state of a trap. Also, for low-$\mathbf{v}_0$ and low-q operation, the trap frequency ν_m is coordination number independent. In addition, traps with the same coordination number are, by definition, identical. Thus if one desires to operate with only one qubit per site, this system is ideally suited.

Further, the ground state of the effective harmonic oscillator trap for the 3-D ion trap configuration is nondegenerate. However, for the center-of-mass oscillations, the excited states in the symmetric operation mode of the trap exhibit degeneracy. Thus the usual cooling mechanisms (laser and sideband) essential for the population of the ground vibrational state of the trap with the ion(s) are unchanged. In addition, deterministic numbers of ions can be loaded per lattice site in the ground state. In the specific case of two ions per trap cell, the key to entangling them or performing gate operations with existing protocols [22] may depend on the heating rate of the ions from their ground state in the trap. The heating rate has not been evaluated in the present work. The present ion trap has a point rf node, as opposed to the linear rf node of the more conventional linear Paul trap geometries that are currently in use for quantum information processing. Thus, the feasibility of usable two-/multi-ion entanglement in the proposed configuration bears further investigation. Another difference which arises due to the high symmetry is an overall rotational motion about the center of mass of the trapped ions, which, due to the distance between two ions in the trap ground state (several micrometers), is very slow ($\approx$1 Hz) compared with other relevant time constants in such systems. If many-particle entanglement can be proven for this structure, either with present-day technology or with a protocol or system yet to be developed, scaling will naturally follow. The fact that, by asymmetric application of either constant or rf voltage, the trap degeneracy can be lifted for the excited states offers other degrees of freedom for exploitation in the future. Thus the LIT offers a new architecture for quantum information processing with ions [15].

Another rich area of study with the 3-D ion trap is the experimental few-body problem. The present-day ability to load a controlled number of atoms, molecules or ions in the lowest-energy states of traps allows attempts at quantitative studies with these very challenging systems. Linear Paul traps have long supported ion crystals which order in shells about the trap axis [23–25]. The 3-D ion trap would fill in a three-dimensionally symmetric fashion. Problems such as minimum energy configurations, phonon mode excitations and crystal relaxation, rotations, and effect of trap symmetry and its changes can be probed. The symmetry of the present trap can be dramatically altered from a totally symmetric to a completely asymmetric configuration (i.e., $\nu_{m;x} = \nu_{m;y} = \nu_{m;z} \leftrightarrow \nu_{m;x} \neq \nu_{m;y} \neq \nu_{m;z}$) with small differences in electrode voltages. In the highly asymmetric configuration the system can be driven into chaotic behavior as evident from single, trapped ion trajectory simulations, which exhibit a dense power spectrum. The ability to catch the ion signal in fluorescence makes trapped ions the natural choice for mapping both the equilibrium configurations and the dynamics of a system of a few, bound particles. Such studies with trapped ions are relevant across disciplines in physics.

In conclusion, the concept of the ion trap described here is versatile and suitable for many experiments over and above [26] those discussed here. The trap operating parameters determined here are easily scaled for different Q/M and trap dimensions. Its primary strengths lie in the ease with which multiple, identical ion traps can be realized and the ability to adapt the trap symmetry to a specific problem without additional experimental complexity.

[1] H. Dehmelt, Rev. Mod. Phys. Soc. **62**, 525 (1990).
[2] W. Paul, Rev. Mod. Phys. Soc. **62**, 531 (1990).
[3] K. Blaum, Phys. Rep. **425**, 1 (2006).
[4] R. E. March and J. J. F. Todd, *Quadrupole Ion Trap Mass Spectroscopy* (Wiley, New York, 2005).
[5] T. Rosenband *et al.*, Science **319**, 1808 (2008).
[6] R. Blatt and D. Wineland, Nature **453**, 1008 (2008).
[7] F. G. Major, V. Gheorghe, and G. Werth, *Charged Particle Traps* (Springer, Heidelberg, 2004).
[8] F. Diedrich *et al.*, Phys. Rev. Lett. **59**, 2931 (1987).
[9] D. J. Wineland *et al.*, Phys. Rev. Lett. **59**, 2935 (1987).
[10] K. Mølhave and M. Drewsen, Phys. Rev. A **62**, 011401(R) (2000).
[11] M. D. Barrett *et al.*, Nature **429**, 737 (2004).
[12] G. Gabrielse and F. C. MacKintosh, Int. J. Mass. Spec. Ion Proc. **57**, 1 (1984).
[13] M. Drewsen and A. Brøner, Phys. Rev. A **62**, 045401 (2000).
[14] W. K. Hensinger *et al.*, Appl. Phys. Lett. **88**, 034101 (2006).
[15] D. Kielpinski, C. Monroe, and D. J. Wineland, Nature **417**, 709 (2002).
[16] S. Seidelin *et al.*, Phys. Rev. Lett. **96**, 253003 (2006).
[17] S. Stahl *et al.*, Eur. Phys. J. D **32**, 139 (2005).
[18] F. G. Major, J. Phys. Lett. **38**, 221 (1977).
[19] Y. Onoda, Master's thesis, Kochi University of Technology, 2006.
[20] D. Hucul *et al.*, Quant. Inf. Comp. **8**, 0501 (2008).
[21] R. F. Wuerker, H. M. Goldenberg, and R. V. Langmuir, J. Appl. Phys. **30**, 441 (1959).
[22] J. I. Cirac and P. Zoller, Phys. Rev. Lett. **74**, 4091 (1995).
[23] W. Alt, M. Block, P. Seibert, and G. Werth, Phys. Rev. A **58**, R23 (1998).
[24] M. Block *et al.*, J. Phys. B **33**, L375 (2000).
[25] J. P. Schiffer, M. Drewsen, J. S. Hangst, and L. Hornekaer, Proc. Natl. Acad. Sci. USA **97**, 10697 (2000).
[26] X.-L. Deng, D. Porras, and J. I. Cirac, Phys. Rev. A **72**, 063407 (2005).